Langmuir

ARTICLE

pubs.acs.org/Langmuir

Unique Properties of Bubbles and Foam Films Stabilized by HFBII Hydrophobin

Elka S. Basheva,[†] Peter A. Kralchevsky,*[,†] Nikolay C. Christov,[†] Krassimir D. Danov,[†] Simeon D. Stoyanov,[‡] Theodorus B. J. Blijdenstein,[‡] Hyun-Jung Kim,[‡] Eddie G. Pelan,[‡] and Alex Lips[§]

[†]Department of Chemical Engineering, Faculty of Chemistry, Sofia University, 1164 Sofia, Bulgaria

[‡]Unilever Research & Development, 3133AT Vlaardingen, The Netherlands

[§]Unilever Research & Development, Port Sunlight, Wirral, Merseyside CH63 3JW, U.K.

Supporting Information

ABSTRACT: The HFBII hydrophobin is an amphiphilic protein that can irreversibly adsorb at the air/water interface. The formed protein monolayers can reach a state of two-dimensional elastic solid that exhibits a high mechanical strength as compared to adsorption layers of typical amphiphilic proteins. Bubbles formed in HFBII solutions preserve the nonspherical shape they had at the moment of solidification of their surfaces. The stirring of HFBII solutions leads to the formation of many bubbles of micrometer size. Measuring the electrophoretic mobility of such bubbles, the ζ-potential was determined. Upon compression, the HFBII monolayers form periodic wrinkles of wavelength 11.5 μm, which corresponds to bending elasticity $k_c = 1.1 \times 10^{-19}$ J. The wrinkled hydrophobin monolayers are close to a tension-free state, which prevents the Ostwald ripening and provides bubble longevity in HFBII stabilized foams. Films formed between two bubbles are studied by experiments in a capillary cell. In the absence of added electrolyte, the films are electrostatically stabilized. The appearance of protein aggregates is enhanced with the increase of the HFBII and electrolyte concentrations and at pH close to the isoelectric point. When the aggregate concentration is not too high (to block the film thinning), the films reach a state with 12 nm uniform thickness, which corresponds to two surface monolayers plus HFBII tetramers sandwiched between them. In water, the HFBII molecules can stick to each other not only by their hydrophobic moieties but also by their hydrophilic parts. The latter leads to the attachment of HFBII aggregates such as dimers, tetramers, and bigger ones to the interfacial adsorption monolayers, which provides additional stabilization of the liquid films.

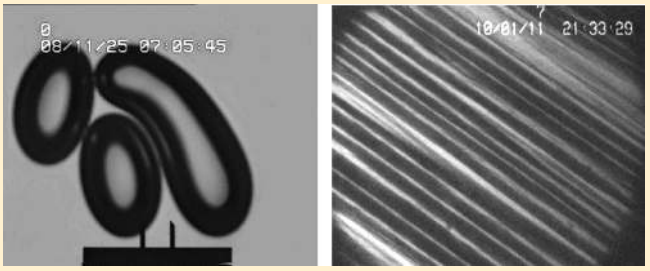

1. INTRODUCTION

The hydrophobins are a class of relatively small cysteine-rich proteins composed of ca. 100 amino acids. They are produced by filamentous fungi, including the well-known button mushrooms.[1−3] The hydrophobin molecules are amphiphilic: they have distinct hydrophobic and hydrophilic parts like surfactant molecules and Janus particles.[4,5] For this reason, the hydrophobins spontaneously adsorb at the air/water interface, where they self-assemble in elastic adsorption layers (membranes) of high mechanical strength as compared to adsorption layers from other proteins. In nature, these self-assembled films coat fungal structures and mediate their attachment to surfaces. The special properties of hydrophobins can find (and have already found) various applications in adhesion and immobilization of functional molecules at surfaces,[6−10] as coating agents for surface modification,[8,9,11,12] and as stabilizers of foams and emulsions.[4,5,13,14] Detailed reviews can be found in refs 1−3.

The hydrophobins are divided into two classes: The molecules of class I form aggregates, which are highly insoluble in water, whereas those of class II form water-soluble aggregates.[3,15] Hydrophobins from the fungus *Trichoderma reesei* have been extensively studied during the past 10 years. From this fungus, three types of class II hydrophobins have been isolated, purified, and characterized: HFBI, HFBII,[16,17] and HFBIII.[18] In aqueous solutions, the class II hydrophobins form dimers (at low concentrations), whereas tetramers are the dominant assemblies at mg/mL concentrations.[19−22] The aggregation in hydrophobin solutions has been studied by light scattering,[4,23] X-ray scattering, and size-exclusion chromatography.[2,18,19,21,24]

The hydrophobins are stable proteins. They have been heated to 90 °C in aqueous solution for at least 15 min without any sign of denaturing.[3,25] The self-assembly of HFBI and HFBII at an air/water interface is not accompanied by changes in their secondary structure and ultrastructure.[22,25] The measured thickness of their adsorption layers indicates that they form *monolayers* at the surface of water.[22,26] The structure of HFBII (the protein used in the present study), determined from crystallized

Received: August 24, 2010
Published: February 14, 2011

samples,[27] shows that it is a single domain protein with dimensions of 24 × 27 × 30 Å. The investigations of HFBI and HFBII films transferred on a solid substrate show that they represent ordered arrays that have a lattice cell, which is larger than the molecular size.[22,24,27] The monolayers of both these hydrophobins contain six molecules in the unit cell of the formed two-dimensional crystal.[22] This special structure could be the main reason for the extraordinary mechanical strength of the hydrophobin monomolecular films (membranes) (see section 3.1).

In summary, HFBII is a protein that has recently been isolated and that shows interesting properties which are not commonly observed for other proteins. Here, our goal is to present an overview of the properties of bubbles and liquid films stabilized by HFBII, based on new and original experimental results for the properties of HFBII adsorption layers and the interactions between them. Interpretation and possible explanations of some of the observed effects are proposed.

The paper is organized as follows. In section 2, the used materials and methods are described. Further, it is demonstrated that due to its high mechanical strength, a solidified monolayer of HFBII can stabilize the irregular (nonspherical) shape of macroscopic bubbles (section 3.1). HFBII stabilizes also microscopic bubbles that spontaneously appear in the protein solutions upon shaking. Because of that, the respective solutions look turbid (section 3.2). Such dispersions of HFBII-covered microbubbles represent a convenient object for electrophoretic ζ-potential measurements, which have been carried out at various pH and the results are reported (section 3.3). The leakage of gas leads to a gradual bubble shrinking that ends with a state of wrinkled bubble (wrinkled HFBII monolayer). From the wrinkle wavelength, the bending elasticity of the HFBII monolayer is determined (section 4). Having in mind the results for a single HFBII adsorption layer, the interaction of two such layers (that form a liquid film) is considered, in relation to the interaction between two bubbles upon contact. The effects of several factors (surface age, pH, and added electrolytes) are experimentally investigated (section 5 and Appendix A). In these experiments, an interesting phenomenon is discovered: the spontaneous formation of a 6 nm thick "S-bilayer", which brings additional information about the adhesive properties of the HFBII molecules (section 5.3). A detailed investigation of the latter phenomenon will be reported in a subsequent paper.[28]

2. EXPERIMENTAL SECTION

2.1. Materials and Methods. In all experiments, HFBII samples produced from yeast fermentation and purified according to a procedure described in detail elsewhere were used.[29] Briefly, *Saccharomyces cerevisiae* strain CEN.PK338 (gal1:URA3, leu2, ura3, pmt1) carried a multicopy integration vector, integrated at the rDNA locus, containing the protein coding sequence of *Trichoderma reesei* HFBII,[17] linked to the *S. cerevisiae* SUC2 signal sequence and under control of the GAL7 promoter and leu2d selectable marker to maintain a high copy number.[30] The strain was grown in 10 L fed batch fermentations as described by Thomassen et al.[31] The cells were removed by centrifugation and filtration over a 0.2 μm filter, and the supernatant containing the HFBII was freeze-dried.

Three HFBII samples supplied by Unilever R&D, Colworth, UK, were used in our experiments. Sample 1 is an aqueous solution of 0.34 wt % HFBII. Sample 2 is a dry powder of HFBII. Sample 3 is an aqueous solution of 2.94 wt % HFBII. Samples 2 and 3 were used only in the electrophoretic experiments to check whether the measured ζ-potential is the same for different samples, which might have different degrees of purity and differences in the procedures of pretreatment and storage. Sample 1 was used in all other experiments. To vary the pH of the investigated solutions, we used NaOH and HCl. The ionic strength was varied by dissolution of different electrolytes: NaCl (Merck), $CaCl_2$ (Fluka), and trisodium citrate (Na_3Citrate). The working temperature was 25 °C.

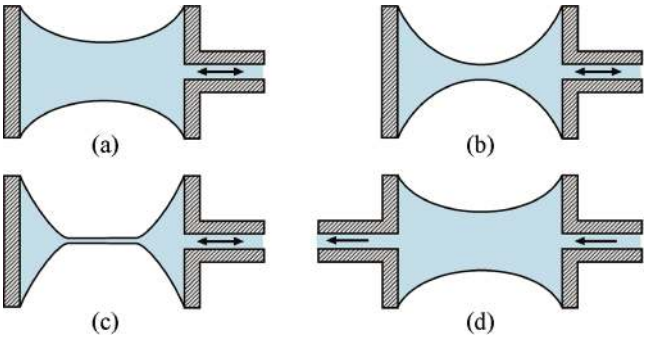

Figure 1. (a) In the SE cell,[32,33] first a biconcave drop is loaded. (b) The distance between the two menisci can be varies by sucking or injection of liquid through the side capillary. (c) Foam film formed in the central part of the cell. (d) After formation of adsorption layers at the two menisci, the flush cell[34] with two side capillaries allows one to change the solution in the cell.

The ζ-potential of the bubbles was measured by Zetasizer 2c (Malvern Instruments) in PC1 experimental cell. The solutions' pH was determined by a Hanna Instruments pH meter in combination with a glass electrode HI 1330B. Two types of electrophoretic measurements were carried out. First, we measured the ζ-potential of HFBII aggregates that spontaneously appear in the solutions of this protein. Second, we measured the ζ-potential of air bubbles covered by HFBII adsorption layers. In both type of measurements, 0.01 wt % aqueous HFBII solutions were used. The micrometer-sized bubbles were formed by dispersing air with the help of Ultra-Turrax T25 (IKA) with a dispersing tool S25N-10G. The pH values before and after the dispersion of air are slightly different because of the dissolution of CO_2 from the bubbles. The ζ-potential of the bubbles has to be plotted vs the pH values measured after the dispersion of air because this is the actual pH in the presence of bubbles.

In the experiments with individual foam films, the Scheludko−Exerowa capillary cell (SE cell)[32,33] and the flush cell by Wierenga et al.[34] were used. Their operational principle is explained in Figure 1. First, the investigated solution is loaded in a cylindrical glass cell (capillary) through an orifice in its wall (Figure 1a). Thus, a biconcave drop is formed inside the capillary, which inner radius was R = 1.2 mm in our experiments. Next, liquid is sucked through the orifice and the two menisci approach each other (Figure 1b) until a liquid film is formed in the central part of the cell (Figure 1c). By injecting or sucking liquid through the orifice, one can vary the radius of the formed film, which thickness can be determined by means of an interferometric method.[32,33]

The flush cell[34] has a second capillary in the wall (Figure 1d). Thus, one can form a biconcave drop from a given solution allowing adsorption layers from a given amphiphile to be formed at the drop surface. Next, the cell interior is flushed by another solution which is supplied by one of the two side capillaries, whereas the liquid is sucked out with the same rate through the second capillary. In our experiments, first a HFBII solution was loaded inside the cell to allow HFBII adsorption at the two menisci, and then this solution was exchanged with water, thus removing the HFBII aggregates from the bulk of the cell. The purpose was to see how important is the presence of HFBII aggregates for the interaction between the two protein adsorption layers. The flushing was carried out in a stepwise manner by supplying small portions (of 80 μL each) of the

new solution through the first capillary simultaneously sucking the same volume of liquid through the second capillary. The volume of the liquid in the side capillaries is about 400 μL, which is ~10 times the volume of the liquid contained in the film holder (40 μL).

2.2. Experimental Procedures in the SE Cell. Two procedures for film formation in the SE cell were used. First, the film was formed *immediately* after the loading of HFBII solution in the experimental cell. This is equivalent to a fast transition from the state in Figure 1a to that in Figure 1c, which is realized within 10−20 s. This procedure will be termed formation of a film with *fresh* surfaces.

The second procedure includes loading of the solution in the experimental cell and waiting for 30 min in a state like that sketched in Figure 1a. During this period of time, adsorption equilibrium between bulk and surface is established, and moreover, the formed HFBII monolayer undergoes a transition from a 2D fluid to an elastic membrane. After this initial period of 30 min, we form the foam film; i.e., we execute the transition from the state in Figure 1a to that in Figure 1c. This procedure will be termed formation of a film with *aged* surfaces.

The experimental cell is placed in a closed container. In this case, the water vapors are equilibrated with the solution, and evaporation from the film is prevented. The experiments under these conditions will be referred as experiments in a *closed cell*.

If the glass cover of the aforementioned container is removed, evaporation of water from the film happens because the humidity of the atmospheric air is well below 100% (typically about 60−75%). In this case, the film becomes considerably thinner and reaches a state, in which it is stabilized by short-range repulsion. The experiments under these conditions will be referred as experiments in an *open cell*.

The reason for the thinning of the foam film in an open cell is the following. The evaporation of water from the film surfaces gives rise to a flow of water from the periphery of the film toward its center. Thus, under steady-state conditions, the following hydrodynamic pressure difference is established between the periphery of the film and its center:[35]

$$\Delta P = \frac{3\eta V_1 j_e}{h^3} r_c^2 \quad (1)$$

Here, η is the dynamic viscosity of the liquid, j_e is the number of water molecules evaporating per unit time from unit area of the film surface, V_1 is the volume per water molecule in the liquid phase, h is the width of the gap in which the fluid flow takes place, and r_c is the film radius (the radius of the contact line at the film periphery). For typical parameter values, $j_e \approx 6 \times 10^{21}$ m^{-2} s^{-1},[36] $r_c = 150\,\mu$m, $h = 30$ nm, $V_1 = 30$ Å^2, and $\eta = 0.001$ Pa s, eq 1 yields

$$\Delta P = 4.5 \times 10^5 \text{ Pa} \quad (2)$$

i.e., about 4.5 atm, which is really a considerable effect. ΔP presses the two film surfaces against each other and is able to overcome the barrier due to electrostatic double-layer repulsion (see the ζ-potential data below).

3. EXPERIMENTS WITH BUBBLES IN HFBII SOLUTIONS

3.1. Bubbles below the Air/Water Interface. Each bubble is released in the bulk of solution from the tip of a capillary. After that, under the action of buoyancy, it moves upward (for about 1 s) until it reaches the air/water interface, where the bubble stops and a liquid film is eventually formed in its upper part. In these experiments, we used 0.005 wt % solutions of HFBII containing 25 mM added $CaCl_2$ at pH = 5.2, which is the natural pH of the solution.

We observed an interesting phenomenon: the formed bubbles were not spherical but had irregular elongated and/or curved

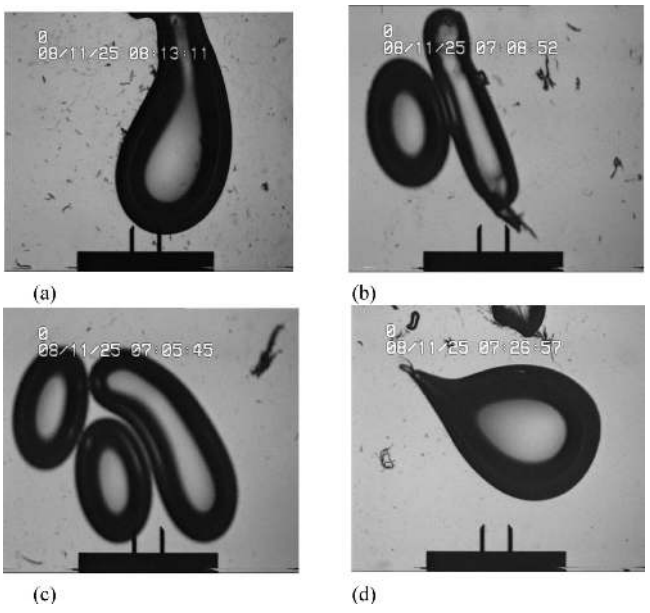

Figure 2. Photographs of millimeter-sized bubbles formed resting below the surface of a 0.005 wt % HFBII solution containing added 25 mM $CaCl_2$. The photos are taken in transmitted light. The reference distance is 400 μm.

shapes. This is illustrated in Figure 2, which shows video frames taken from above in transmitted light. The microscope magnification is 2.5×, and the length of the reference distance is 400 μm.

The nonspherical bubble shapes (Figure 2) can be explained with solidification of the HFBII adsorption layer. In other words, the dense monolayer of HFBII undergoes a transition to two-dimensional elastic solid ("skin"), which possesses *shear elasticity*. Each bubble preserves its instantaneous shape at the moment of solidification of its surface. It is amazing that a protein layer of thickness 3 nm determines the shape of 3 mm large bubbles. In other words, the HFBII adsorption layers exhibit a unique mechanical strength.

A possible reason for that could be the structure of the HFBII monolayer, which consists of cells with six molecules[22] resembling the structure of the graphene sheet, which is known for its mechanical strength.[37−39] (Typical amphiphilic proteins, such as β-casein, β-lactoglobulin, and bovine serum albumin, do not form such structure.) This structural analogy deserves to be further investigated; the rodlets observed in some experiments[3] may turn out to be hydrophobin tubules.

As known, a material that behaves as a solid under low applied stresses may start to flow above a certain level of stress, called the *yield stress* of this material.[40−43] The fact that a HFBII monolayer can solidify (as evidenced by the nonspherical bubbles in Figure 2) but undergo a transition to viscoelastic layer when subjected to shear deformation (see Figure B1 in Appendix B) indicates that the HFBII monolayer is characterized by a certain yield stress, which can be a subject of subsequent rheological studies.

Shear elasticity has been registered also for typical proteins, like β-lactoglobulin[44] and lysozyme.[45] However, the bubbles formed in the solutions of the latter proteins are spherical. This can be due to a relatively low yield stress. In contrast, the shapes of the bubbles in Figure 2 indicate that for hydrophobins the yield stress is considerably higher than for the other investigated

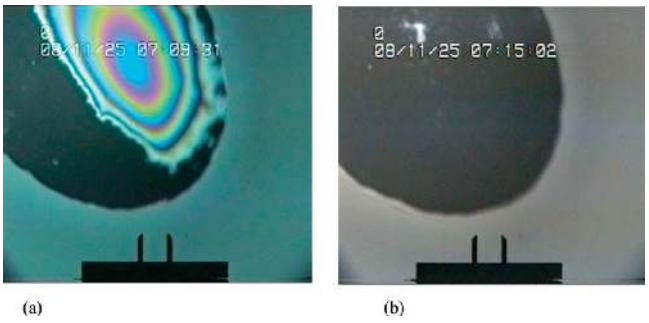

Figure 3. Photographs of the thin liquid films formed at the upper part of the bubbles pressed by buoyancy force against the solution/air interface (0.005 wt % HFBII + 25 mM $CaCl_2$). (a) Initially, the film is thicker and contains a dimple. (b) Subsequently, the dimple flows out and a film of uniform thickness is formed.

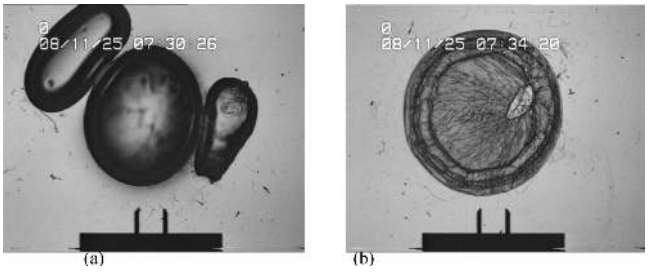

Figure 4. In few cases we observed rupture of the thin film in the upper part of the bubble. After the rupture, the HFBII skin of the bubble remains in the solution near its surface. (a) Before the rupturing of the film of the central bubble and (b) after the film rupturing. The reference distance is 400 μm.

proteins. These results imply that rheological properties of HFBII adsorption layers, such as shear and dilatational elasticity[4,14] and yield stress,[43] essentially influence the mechanical behavior of HFBII stabilized dispersions.

To see the film in the upper part of a bubble, like those in Figure 2, we carried out observations in reflected light at a higher magnification. Photos of such a film are shown in Figure 3. The film thins gradually and finally a state of uniform thickness is reached. A sharp transition to S-bilayer is not observed as with films in the SE cell (see section 5.3). At concentration 0.005 wt % HFBII, the films formed at the top of the bubbles are stable. In experiments with 500 bubbles, only two cases of film rupturing happened. One of them is shown in Figure 4. After the film breakage, the HFBII skin of the bubble remains.

Observations of bubbles in HFBII solutions at temperatures in the range 25−55 °C were carried out. The bubbles preserve their nonspherical shape in the whole investigated temperature range; i.e., their shapes are not sensitive to temperature. In other words, indications for fluidization of the HFBII adsorption layer were not found in this temperature interval.

Nonspherical bubbles (like those in Figure 2) were observed in HFBII solutions that do not contain added electrolytes or contain NaCl at various concentrations. The presence of electrolyte is not a necessary condition for the formation of nonspherical bubbles.

3.2. Turbidity of the HFBII Solutions. Upon shaking, an initially clear HFBII solution becomes turbid. If the turbid solution is treated by ultrasound (sonicated), it becomes transparent again. Microscopic observations of the turbid solutions (Figure 5) indicate that they contain micrometer-sized particles that look like the irregularly shaped bubbles in Figure 2 but are much smaller. Hence, the turbidity of these solutions can be explained with the formation of HFBII-stabilized bubbles upon shaking. The turbidity is due to the substantial difference between the refractive indexes of the protein solution and the air in the bubbles. The sonication destroys the bubbles, and the solutions become clear again.

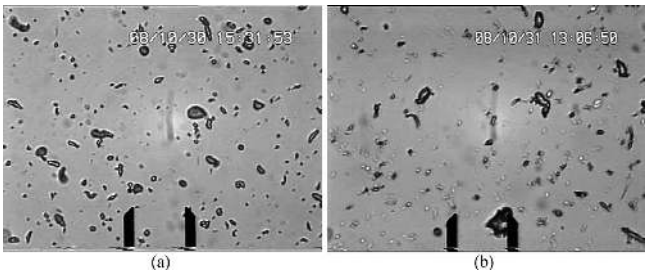

Figure 5. Photographs of 0.01 wt % HFBII solutions stirred by Ultra-Turrax; the reference mark is 20 μm. In the bulk of solution, we observe irregularly shaped bubbles. The Zetasizer gives the ζ-potential of these bubbles. The shape and size of the bubbles are similar at the two examined pH values: (a) pH = 3.6 (adjusted by citric acid) and (b) pH = 8.4 (adjusted by NaOH).

It should be noted that even the clear solutions contain HFBII tetramers of size ca. 6 nm, which are invisible by optical microscopy and do not contribute to turbidity. Upon aging of the solutions, or upon addition of electrolyte, the tetramers form bigger HFBII aggregates (from 100 nm to several μm), which are seen in the investigated foam films and at the solution's surface by microscope (see section 5.2 and Figures A13 and A14 in Appendix A). Note, however, that with naked eye the solutions that contain such aggregates look transparent due to the used rather low HFBII concentrations, 0.005−0.01 wt %. From this viewpoint, the turbidity of the investigated solutions after shaking is almost completely due to the formed HFBII-stabilized bubbles, which have a much greater volume fraction than that of the protein.

3.3. ζ-Potential Measurements. We used bubbles formed in the HFBII solutions to measure their ζ-potential as a function of pH. The experimental procedure is as follows. First, we prepared a solution of 0.01 wt % HFBII. After that, we divided the solution in portions of 10 mL and adjusted the pH of each of them with minimal amounts of NaOH and HCl. We put about 5 mL from the solution in a glass cylinder of diameter 16 mm and height 95 mm and subjected it to sonication for few seconds in ultrasonic bath until the solution became clear. Then, we dispersed air in the solution by means of Ultra-Turrax, using a dispersing tool of diameter 10 mm, at 24 000 rpm, for about 15−20 s. The obtained turbid solution is sucked from the bottom of the cylinder by a syringe with a needle and is inserted in the Zetasizer. The measurements were made as quick as possible to avoid the emergence of the air bubbles under the action of buoyancy. The procedure was repeated with the second portion of 5 mL from the initial solution to check the reproducibility of the measurement.

We carried out also electrophoretic experiments with HFBII aggregates. The 0.01 wt % HFBII solutions were again subjected to sonication for few seconds until they became clear. After 15 min, micrometer-sized (and smaller) HFBII aggregates spontaneously appear in the solution. Their ζ-potential was measured.

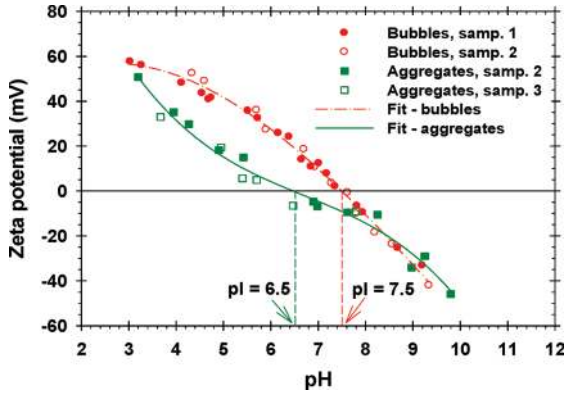

Figure 6. Experimental pH dependence of the ζ-potential of bubbles and aggregates in 0.01 wt % HFBII solutions at 25 °C for different protein samples denoted in the figure (details in the text). The fits by cubic polynomials are guides to the eye.

In Figure 6, the results for the ζ-potential measured with aggregates and bubbles are compared. The data obtained with different samples of HFBII practically coincide, which means that the results are not affected by differences in the procedures of HFBII pretreatment. For aggregates, the isoelectric point is pI ≈ 6.5, which is very close to the value 6.7 calculated by the program ProtParam based on the protein primary structure data.[46,21] For pH > 8, the ζ-potential values coincide for bubbles and aggregates (Figure 6). However, for 3 < pH < 8, the ζ-potential of HFBII-covered bubbles is systematically higher than those of the aggregates, and pI ≈ 7.5 for bubbles. This difference between the ζ-potential of aggregates and bubbles can be explained by the fact that in the dense HFBII adsorption layers covering the bubbles only about 1/6 of the surface of the protein molecules is in contact with water, and functional groups only on this contact surface are expected to be ionized.

Change in the isoelectric point upon adsorption was found also for the protein β-lactoglobulin (BLG).[47] Experiments with emulsion films (oil/water/oil) stabilized by BLG showed that the isoelectric point is changed from pI = 5.2 in the bulk to pI = 4 in the film. Therefore, it seems that the conformational changes, which accompany the BLG adsorption, lead to a shift in the isoelectric point.[47,48] As mentioned above, in the case of HFBII the shift in pI could be explained with embedding of a part of the ionizable groups in the closely packed protein adsorption layer, rather than with conformational changes upon adsorption.

4. WRINKLING OF HFBII ADSORPTION LAYERS AND THEIR BENDING ELASTICITY

4.1. Experimental Observation of Wrinkles. If an elastic membrane is subjected to compression, at a given stage of compression it forms wrinkles (ripples). This was observed with phospholipid monolayers and trilayers,[49] surface metal−organic complexes,[50] surfactant layers in concentric lamellar phases,[51] and monolayers of nanoparticles in a Langmuir trough.[52] Such periodic wrinkles have been observed also on the surface of bubbles[4] and sessile drops[26] covered by adsorption layers of hydrophobin and on spread monolayers of HFBII.[14]

From the wavelength of the wrinkles, one can determine the bending elasticity (rigidity), k_c, of the adsorption layer.[53] For this goal, we took photographs of wrinkles formed on the surface of

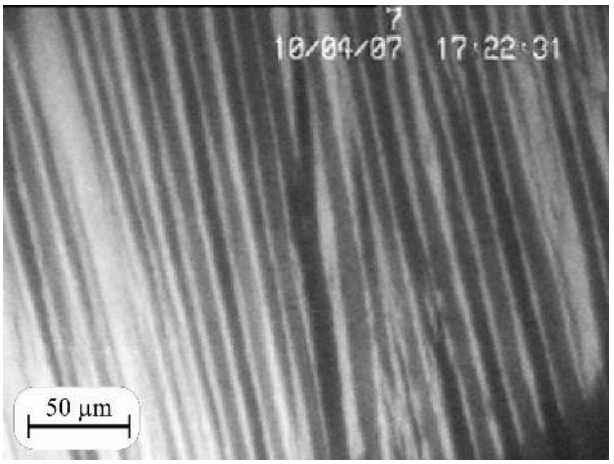

Figure 7. Photograph of wrinkles in an HFBII adsorption layer subjected to compression; air/water interface; the aqueous phase is a solution of 0.005 wt % HFBII with 0.01 M added NaCl.

the investigated HFBII solutions. The wrinkles were obtained by using the SE cell (Figure 1) in the following way.

The biconcave drop in the SE cell was kept for 15 min in a state close to that in Figure 1b. Then, we injected solution through the orifice in the wall, and the meniscus acquired a shape like that in Figure 1a. This transition is accompanied by diminishing of the macroscopic surface area. The degree of surface compression can be controlled by the amount of injected solution. The compression leads to the appearance of wrinkles in the protein adsorption layer; a typical photograph is shown in Figure 7. As seen in the figure, domains with parallel periodic ripples are observed. Their wavelength, λ, is practically the same for different periodic domains, and it does not change with time, although the compressed membrane gradually relaxes (within 5−6 min): the amplitude of wrinkles decreases; flat regions appear and grow between the wrinkled domains. The relaxation of the wrinkles can be explained with a slow motion of the three-phase contact line along the inner wall of the cell (which is equivalent to a decrease in the degree of monolayer compression) rather than to desorption of HFBII molecules. (In reality, the contact line is not fixed to the edge, as sketched in Figure 1a, but it is free to move along the inner wall of the glass cell.)

4.2. Interpretation of the Observed Pattern. Just like an elastic spring, a membrane may have either positive or negative tension when it is subjected to stretching or compression, respectively. The tension-free state (of zero tension) is in the middle between the aforementioned two regimes. However, the membrane possesses an additional degree of freedom—to bend. In the region of negative membrane tensions, it is energetically more favorable the membrane to bend instead of to decrease its area upon compression.[53] This is the reason for the appearance of wrinkles. The bending elasticity (rigidity), k_c, determines the wavelength, λ, of the formed wrinkles. The values of k_c can be obtained from the experimentally measured λ by means of the formula[53]

$$k_c = \frac{\Delta\rho g \lambda^4}{16\pi^4} \qquad (3)$$

where $\Delta\rho$ is the difference between the mass densities of the two adjacent fluid phases and g is the acceleration due to gravity. Furthermore, the membrane tension in the wrinkled state can be

determined from the expression

$$\sigma_m = -(4k_c g\Delta\rho)^{1/2} \quad (4)$$

Here, σ_m is the thermodynamic tension of the membrane, as defined in ref 53. It should be noted that at a given area of an (almost) incompressible membrane the latter has an additional degree of freedom: to form fewer wrinkles of greater amplitude or to form more wrinkles of smaller amplitude. In ref 53, the energy of the system is minimized with respect to this additional degree of freedom. Equations 3 and 4 correspond to the state of minimal energy, which is observed in the experiment.

It is important to also note that eqs 3 and 4 are valid in the case of small deformations, i.e., $|\nabla\zeta|^2 \ll 1$, where $z = \zeta(x,y)$ is the membrane shape; x, y, and z are Cartesian coordinates, and ∇ is the del operator in the xy-plane. Theoretically, λ is independent of the membrane area and of the degree of compression. In other words, in the linear regime, the compression of the membrane leads to increase in the wrinkling amplitude at constant wavelength, λ, which is in agreement with our experimental observations.

Processing the image in Figure 7 and in six other photographs taken under similar conditions, we obtained that the average wavelength of the wrinkles in the HFBII layers is $\lambda = 11.5 \pm 0.1$ μm. Using this value as well as $\Delta\rho = 1000$ kg/m^3 and $g = 9.807$ m/s^2, from eqs 3 and 4 we calculate

$$k_c = 1.1 \times 10^{-19}\ \text{J}, \quad \sigma_m = -6.6 \times 10^{-5}\ \text{mN/m} \quad (5)$$

The latter value of k_c is close to the bending elasticity of bilayer phospholipid membranes.[54−56] The obtained small value of σ_m means that the wrinkling occurs at a very low negative membrane tension, close to the tension-free state (that with $\sigma_m = 0$).

In Figure 2K of ref 26, the average wrinkling wavelength of a HFBI adsorption layer is $\lambda = 33 \pm 3$ μm. Using this value, from eqs 3 and 4 we obtain

$$k_c = (7.5 \pm 0.7) \times 10^{-18}\ \text{J},$$
$$\sigma_m = -5.4 \times 10^{-4}\ \text{mN/m} \quad (6)$$

The latter value of k_c is about 75 times greater than the bending elasticity of bilayer phospholipid membranes. It turns out that for HFBI the bending elasticity is considerably greater than for HFBII; presumably in both cases we are dealing with monolayers. However, for both HFBI and HFBII k_c is much greater than for monolayers from conventional surfactants, for which a compressed monolayer undergoes a collapse (buckling instability), instead of wrinkling.

The term "tension-free state" was introduced by Evans and Skalak[57] in mechanics of phospholipid bilayers and biological membranes. In relation to protein adsorption layers (membranes) we call "tension-free" the state for which $\sigma_m = 0$, where σ_m is the thermodynamic tension as defined in ref 53. Physically, zero tension means that the attractive and repulsive forces acting in the membrane counterbalance each other. However, a tension-free membrane does not lose its mechanical strength. In this state, the stretching, shearing and bending elastic moduli of the membrane can be high and can oppose any deformation like an elastic solid shell.

The pressure difference across the surface of a bubble or drop covered by a HFBII monolayer can be estimated by using the Laplace equation, $\Delta P \approx 2\sigma_m/R$, where R is the average curvature of the membrane.[53] The experimental data in Appendix C, which are obtained by capillary-pressure tensiometry (CPT),[58,59] show that we have $\Delta P \approx 0$ in the wrinkled state in the framework of the experimental accuracy. Indeed, taking $R = 1$ mm along with the value of σ_m from eq 5, we estimate $|\Delta P| = 1.32 \times 10^{-4}$ Pa, which is below the threshold of the experimental accuracy of the CPT method.

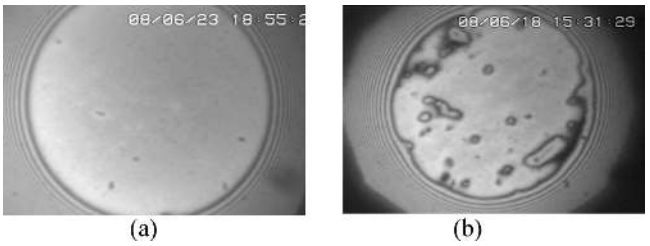

Figure 8. Effect of protein concentration. Foam films stabilized with hydrophobin at concentrations (a) 0.003 wt % HFBII; film lifetime ≈1 min; (b) 0.005 wt % HFBII, about 30 min after the film formation; stable film. No added electrolyte.

From the viewpoint of foam applications, the physical importance of the bending elasticity, k_c, is that it stabilizes the protein adsorption layers on the surface of shrinking bubbles against collapse. In addition, the very low absolute value of the membrane tension, σ_m (see eqs 5 and 6), means that the pressure difference between two neighboring bubbles in the foam will be also very low, almost zero (see also Appendix C). The latter fact means that the foam disproportionation (Ostwald ripening) will be prevented and the foam will be protected against coarsening and destruction.

5. FOAM FILMS FROM HFBII SOLUTIONS

5.1. Foam Films from HFBII Solutions without Added Electrolytes. To study the *effect of protein concentration*, we performed experiments in the concentration range 0.0001−0.1 wt % HFBII for films with fresh interfaces (of age about 20 s) in the absence of any electrolyte at the solutions' natural pH. At concentrations <0.001 wt %, it was impossible to obtain stable films: they ruptured at the moment of their formation.

A sharp transition in the film lifetime (stability/instability) was observed at concentration 0.003 wt % HFBII. Most likely, at this concentration the protein adsorption layer at the film surface undergoes a transition from 2D fluid to 2D elastic body (membrane), i.e. the protein forms a skin at the air/water interface. At this concentration, relatively uniform thick films (thickness between 80 and 100 nm) are formed. Sometimes, small aggregates can be seen in the film or in the surrounding meniscus (Figure 8a). The film stability increases with the further increase of protein concentration. At concentration 0.005 wt % HFBII, the films are stable. Thirty minutes after their formation, many aggregates are seen in the films (Figure 8b).

Effect of Surface Age. As a rule, the aging of the HFBII adsorption layers at the air−water interfaces (before the film formation) results in a longer film lifetime (increased stability) and in the appearance of more aggregates (see Figure 9). The stabilizing effect of surface aging is most probably due to the formation of mechanically strong elastic protein membrane at the two film surfaces and to the additional steric effect of sandwiched protein aggregates. In general, the ability of proteins to generate repulsive interactions (e.g., steric and electrostatic) in the liquid films and to form an interfacial membrane that is

dx.doi.org/10.1021/la104726w |*Langmuir* 2011, 27, 2382–2392

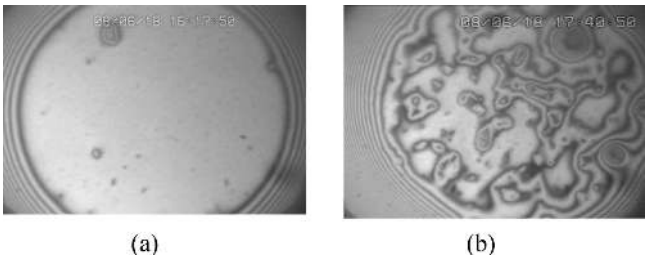

Figure 9. Effect of surface age: Foam films from 0.01 wt % HFBII solutions; no added electrolyte; closed cell. (a) Film with fresh surfaces—several aggregates are seen. (b) Film with aged (for 30 min) surfaces—much more aggregates are seen.

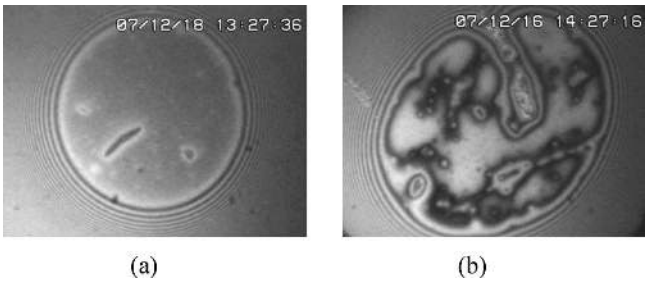

Figure 10. Effect of pH: Foam films of aged (for 30 min) surfaces formed from 0.1 wt % HFBII solutions without added electrolyte; closed cell. (a) pH = 3.5; (b) pH = 6.3.

resistant to rupture plays an important role in stabilizing bubbles in foams or droplets in emulsions against coalescence during long-term storage.[60,61]

Effect of pH. Figure 10 (0.1 wt % HFBII) illustrates that at pH = 3.5 much less aggregates are seen in the film than for pH = 6.3. This result is consistent with the ζ-potential vs pH plot in Figure 6. Indeed, at pH = 3.5 the positive ζ-potential is about 2 times greater than that at pH = 6.3. In other words, the decreased electrostatic (double layer) repulsion at the higher pH (closer to the isoelectric point) leads to the appearance of larger aggregates. In general, the presence of aggregates leads to stabilization of liquid films from protein solutions.[62−67]

At pH = 3.5 and at a lower protein concentration, 0.003 wt % HFBII, after 5 min surface aging the films are stable (lifetime longer than 30 min), and no aggregates are seen in them. Under the same conditions, but after 30 and 60 min aging the films ruptured at the moment of their formation. A possible explanation for such film behavior could be that at longer times the adsorbed HFBII molecules form interfacial "islands" with relatively large free spaces between them; the overlap of such free (unprotected) spaces on the two opposite surfaces upon the film formation may result in film rupture. At higher protein concentrations (Figure 10), such spaces are missing and the films are stable, which can be also due to the steric effect of the sandwiched aggregates.

5.2. Effect of Added Electrolytes. We studied the effect of three electrolytes: NaCl, $CaCl_2$, and Na_3Citrate. Detailed information on the effect of these electrolytes on the foam films from HFBII solutions is given in Appendix A. Here, we summarize and illustrate the most important results of these experiments.

In the absence of added electrolyte, the films with fresh surfaces have a thickness of about 80 nm, which indicates electrostatic stabilization (see data for the ζ-potential in

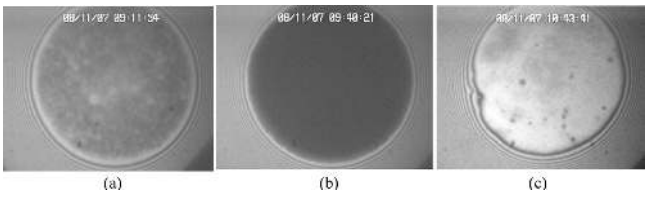

Figure 11. Foam film from 0.005 wt % HFBII solution in the presence of 60 mM NaCl: (a) Fresh surfaces, closed cell; many aggregates in the film. (b) Fresh surfaces, open cell: the aggregates are driven out of the film; its thickness becomes 12 nm. (c) Aged surfaces: thick film with aggregates; the same is observed in closed and open cell.

Figure 6); no aggregates are visible. Aggregates are seen in films with aged surfaces. In both cases (fresh and aged surfaces), the opening of the cell (the evaporation of water from the film surfaces) results in the formation of a stable film of thickness 12 nm. If we try to separate the surfaces of this 12 nm film, we observe increase of the contact angle (hysteresis) in front of the advancing Plateau border. This indicates attractive interaction between the two film surfaces (reversible sticking); see Figures A1 and A2 in Appendix A.

In the presence of electrolyte, the films contain more aggregates, which are trapped in the films and increase their thickness (Figure 11a). In the case of films with *fresh* surfaces, the opening of the experimental cell leads to further thinning of the films. The visible aggregates are driven out of the film, which again reaches a final thickness of 12 nm (Figure 11b). In the case of films with *aged* surfaces, more and larger aggregates are present in the films. The steric hindrance due to these aggregates can prevent the further thinning of the films in both closed and opened cells (Figure 11c).

The above picture is similar for NaCl and $CaCl_2$ at the same ionic strength. It is interesting that in the case of films from HFBII solutions with $CaCl_2$ the equilibrium film thickness is minimal in the range 25−40 mM $CaCl_2$. At lower $CaCl_2$ concentrations, the films are thicker because of the electrostatic repulsion between the two film surfaces (data for the ζ-potential are shown in Figure 6), whereas at higher $CaCl_2$ concentrations the presence of aggregates hinders the film thinning (see Table A3 in Appendix A).

It should be noted that HFBII aggregates are seen not only in foam films but also at single air/water interfaces. This fact indicates that the aggregates are able to adhere to the HFBII monolayer that covers the air/water interface. To check that, we used the flush cell.[34] Initially, a solution of 0.005 wt % HFBII with 0.5 mM Na_3Citrate is loaded in the cell. After aging for 30 min in the state sketched in Figure 1d, the solution between the two menisci (covered with HFBII adsorption layers) is exchanged with an aqueous solution that contains 0.5 mM Na_3Citrate alone. Then, we bring the two menisci into contact, as sketched in Figure 1c. The formed film contains aggregates: The pictures in Figures 11a (no flushing) and 12a (after flushing), showing films with entrapped aggregates, are quite similar. The latter fact indicates that the adsorption of HFBII at the air/water interface is irreversible, at least in the case of not-too-low concentrations, at which the adsorbed molecules are consolidated and form an elastic membrane (skin). Despite the flushing with a Na_3Citrate solution (without HFBII), many of the aggregates remain fixed to the film surfaces and are not carried away by the flow.

5.3. Formation of S-Bilayer. After opening the cell and allowing evaporation from the film, it thins to a final state of

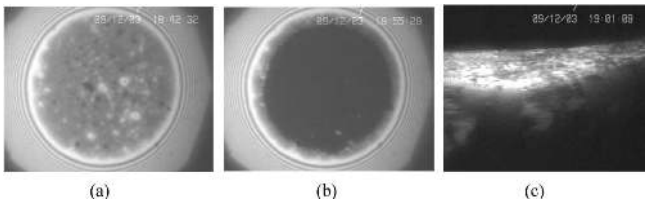

Figure 12. Film from a solution of 0.005 wt % HFBII + 0.5 mM Na_3Citrate (aged surfaces), after the exchange of the protein solution with 0.5 mM Na_3Citrate: (a) 20 min after the film formation we observe a film that contains many aggregates (average thickness 36 nm). (b) In open cell, the aggregates are driven out of the film and its thickness becomes 12 nm. (c) A transition to S-bilayer of thickness ≈6 nm (the black area in the upper part) is observed.

thickness 12 nm without visible aggregates (see Figure 12b). The latter is similar to Figure 11b (no flushing). The difference between the cases with 60 mM NaCl (Figure 11) and 0.5 mM Na_3Citrate (Figure 12) is that in the latter case we observe a subsequent sudden transition from 12 to 6 nm in the film thickness (Figure 12c). Because the dimension of the HFBII molecule along the normal to the interface is ≈3 nm, the film of thickness 6 nm consists of two layers of protein molecules; i.e., it is a self-assembled bilayer (S-bilayer). The latter is a compact membrane of HFBII, which (to some extent) resembles the S-layer—a self-assembled protein monolayer discovered by Messner and Sleytr.[68] In our case, the 6 nm black film appears spontaneously and quickly displaces the thicker film, and during its formation the film area considerably expands: During this transition, the film size increases from a radius of about 100 μm to a radius greater than 1000 μm. For this reason, the border between the S-bilayer (in the upper part of Figure 12c) and the Plateau border looks as a straight line. In other words, this 6 nm thick film appears with a great energy gain.

The experiments indicate that the presence of electrolyte is a necessary condition for the formation of S-bilayers. The electrolyte suppresses the electrostatic barrier that prevents the contact of the two surfaces. Depending on the type of electrolyte, different ionic strengths are necessary for the bilayer formation in SE cell. This effect and other properties of the S-bilayers are investigated in a subsequent study.[28] At higher ionic strengths and/or aged surfaces, the appearance of many aggregates may hinder the thinning of the film and the S-bilayer formation (see e.g. Figure 11c).

6. DISCUSSION

The experiments with HFBII monolayers in a Langmuir trough indicate that the surface pressure of a dense monolayer, just before its wrinkling, is ≈60 mN/m (see e.g. ref 14). Multiplying the latter value with the area per protein, 2.4 × 2.7 = 6.48 nm^2, we obtain 3.89 × 10^{-19} J ≈ 95 kT per molecule. The latter estimate shows that the adsorption energy per HFBII molecule is much greater than the thermal energy kT, which is in agreement with the fact that the adsorption of HFBII at the air−water interface is irreversible; see the discussion of Figure 12a above. To make this estimate, we have assumed that the HFBII adsorption layer is dense. However, it may have voids,[3,26,69] and then the real adsorption energy per molecule could be even greater than 95 kT. This free-energy gain is related to the transfer of the hydrophobic parts of a HFBII molecule from an aqueous to a nonaqueous environment, and therefore it can be considered

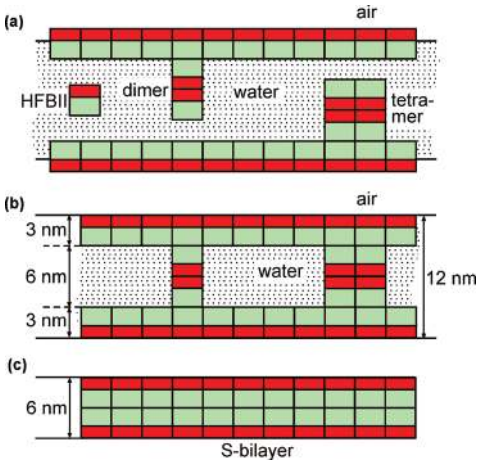

Figure 13. (a) HFBII dimers and tetramers can adhere to the film surfaces owing to the attractive interaction between the *hydrophilic* parts of the HFBII molecules. (b) The adherent aggregates can bridge between the two film surfaces. (c) The same attractive interaction is responsible for the energy gain upon the formation of an S-bilayer. The adherent aggregates (a, b) are incorporated in the growing S-bilayer (c).

as a hydrophobic effect.[70] The formation of HFBII dimers and tetramers in the bulk of solution[19−22] is also due to the hydrophobic interaction.

An adhesive interaction is also observed in the S-bilayers. From the experimental contact angle of S-bilayers,[28] $\theta \approx 51°$, we estimate the adhesive energy per monolayer

$$\Delta W = 2\sigma(1 - \cos\theta) = 8.9\ \text{mN/m} \qquad (7)$$

where we have substituted the surface tension of a dense HFBII monolayer, $\sigma \approx 72-60 = 12$ mN/m (see above). Multiplying ΔW with the area per molecule, 6.48 nm^2, we obtain 5.8 × 10^{-20} J ≈ 14 kT per pair of interacting HFBII molecules. This is the energy of adhesion of two protein molecules belonging to the two opposite surfaces of an S-bilayer (see Figure 13). In this case, the adhesion is between the parts of the HFBII molecules in contact with water, i.e., with its *hydrophilic* parts.

Hence, the experimental results indicate that in water the HFBII molecules behave as sticky particles. Their hydrophobic parts adhere with energy of the order of 95 kT per molecule, whereas their hydrophilic parts stick to each other with an energy gain of ca. 14 kT per pair of molecules. This explains why the hydrophobin forms aggregates and compact adsorption layers (membranes) (see Figures 8−12). In particular, the existence of adhesive interaction between the hydrophilic parts of these protein molecules means that HFBII dimers and tetramers (and bigger aggregates) can stick to the film surfaces, as sketched in Figure 13a. The adherent aggregates can stabilize the liquid films in two ways. They can hinder the thinning of the films (see e.g. Figures 11a and 12a). In addition, if the interfacial film is expanded, they can supply HFBII molecules to repair the integrity of the protein adsorption monolayer by filling the growing voids in the HFBII adsorption monolayers.[3,26,69]

As already mentioned, the estimated attraction energies, which are much greater than the energy of thermal motion, imply that the HFBII molecules have to aggregate in the aqueous solution. This is experimentally observed; for example, such aggregates are seen around the bubbles in Figures 2 and 4.

The attraction between the hydrophilic parts of the protein molecules would lead to the attachment of HFBII aggregates to the monolayer at the air/water interface. This is also observed—by microscope one sees that micrometer-sized fibrillar aggregates come and stick to the solution's surface. Photographs of micrometer-sized aggregates attached to the interfacial protein adsorption layer are shown in Figures A13 and A14 of Appendix A. The experiments by the flush cell described in section 5.2 also confirm the aggregate attachment to the film surfaces.

When a greater force presses the film surfaces against each other, as it happens under open cell condition, the larger HFBII aggregates can be driven out of the film, and the latter reaches a state of thickness h = 12 nm (see Figures 11b and 12b as well as Figures A1c, A2c, A7c, A8b, A10c, and A11c in Appendix A). This state can be interpreted as a film that contains sandwiched HFBII dimers and tetramers that play the role of spacers (Figure 13b).

Upon certain conditions it is possible the foam film to reach its thinnest state of S-bilayer (see Figures 12c and 13c). The experiments show that the formation of an S-bilayer is accompanied by a considerable expansion of the film area. During this process, the HFBII molecules in the entrapped dimers and tetramers (Figure 13b) are most probably incorporated in the expanding surface monolayers.

The main differences between HFBII and the typical amphiphilic proteins, such as β-casein, β-lactoglobulin, and bovine serum albumin (BSA), are in the following two respects:

First, the mechanical stiffness of the HFBII adsorption monolayers is significantly greater than that in the case of typical proteins. For example, the stiffening of the HFBII monolayers leads to the formation of nonspherical bubbles (Figures 2 and 5), whereas the bubbles formed in typical protein solutions are spherical. The stiffening is related to the higher shear elasticity of the HFBII adsorption monolayers. This is illustrated in Appendix B with a comparison of the mechanical responses of adsorption layers from HFBII and β-casein, which are subjected to shearing in a rotational viscometer. Under the same conditions, the HFBII monolayer exhibits viscoelastic behavior dominated by its shear elasticity, whereas the β-casein monolayer behaves as a two-dimensional fluid.

Second, the contact angles measured with HFBII S-bilayers are much greater than the contact angles of liquid films stabilized by typical proteins. For example, the experimental measurements[71] give maximum contact angles 0.9° and 1.4° for aqueous films stabilized, respectively, with 0.015 wt % BSA and 0.01 wt % β-casein in the presence of 150 mM NaCl, whereas the contact angles of the HFBII S-bilayers are ≈50° (for details see ref 28). As noted above, the large contact angles in the case of HFBII indicate a strong attraction between the hydrophilic parts of the HFBII molecules (see eq 7); such effect is absent for typical proteins.

Recently, Wang et al.[72] suggested that the attraction between the hydrophobin and a second layer of hydrophilic protein are due to electrostatic interactions. If this is the case, a possible physicochemical mechanism of the attraction between the hydrophilic parts of protein molecules is provided by the patch−charge interaction.[73]

In summary, HFBII differs from the typical amphiphilic proteins (i) by its ability to form adsorption monolayers of considerable mechanical stiffness and (ii) by the significant energy of attraction between the hydrophilic parts of two HFBII molecules in aqueous solutions.

■ ASSOCIATED CONTENT

Supporting Information. Appendix A: foam films stabilized by HFBII: effect of electrolytes; Appendix B: protein adsorption layers subjected to shearing; Appendix C: pressure difference across a curved HFBII membrane. This material is available free of charge via the Internet at http://pubs.acs.org.

■ AUTHOR INFORMATION

Corresponding Author

*Tel (+359) 2-9625310; Fax (+359) 2-9625643; e-mail pk@lcpe.uni-sofia.bg.

■ ACKNOWLEDGMENT

The authors gratefully acknowledge the support from Unilever Research Institute in Vlaardingen (NL), from the project DO-02-121/2009 of NSF−Bulgaria, and from COST Action D43. John Chapman, Peter Nieuwpoort, and Tim Litchfield are acknowledged for preparation and purification of hydrophobin HFBII.

■ REFERENCES

(1) Wösten, H. A. B. Hydrophobins: multipurpose proteins. *Annu. Rev. Microbiol.* **2001**, *55*, 625–646.

(2) Linder, M. B.; Szilvay, G. R.; Nakari-Setälä, T.; Penttila, M. Hydrophobins: the protein-amphiphiles of filamentous fungi. *FEMS Microbiol. Rev.* **2005**, *29*, 877–896.

(3) Linder, M. B. Hydrophobins: proteins that self assemble at interfaces. *Curr. Opin. Colloid Interface Sci.* **2009**, *14*, 356–363.

(4) Cox, A. R.; Cagnol, F.; Russell, A. B.; Izzard, M. J. Surface properties of class II hydrophobins from *Trichoderma reesei* and influence on bubble stability. *Langmuir* **2007**, *23*, 7995–8002.

(5) Cox, A. R.; Aldred, D. L.; Russell, A. B. Exceptional stability of food foams using class II hydrophobin HFBII. *Food Hydrocolloids* **2009**, *23*, 366–376.

(6) Linder, M. B.; Qiao, M.; Laumen, F.; Selber, K.; Hyytiä, T.; Nakari-Setälä, T.; Penttilä, M. E. Efficient purification of recombinant proteins using hydrophobins as tags in surfactant-based two-phase systems. *Biochemistry* **2004**, *43*, 11873–11882.

(7) Zhao, Z.-X.; Qiao, M.-Q.; Yin, F.; Shao, B.; Wu, B.-Y.; Wang, Y.-Y.; Wang, X.-S.; Qin, X.; Li, S.; Yu, L.; Chen, Q. Amperometric glucose biosensor based on self-assembly hydrophobin with high efficiency of enzyme utilization. *Biosens. Bioelectron.* **2007**, *22*, 3021–3027.

(8) Qin, M.; Wang, L.-K.; Feng, X.-Z.; Yang, Y.-L.; Wang, R.; Wang, C.; Yu, L.; Shao, B.; Qiao, M.-Q. Bioactive surface modification of mica and poly(dimethylsiloxane) with hydrophobins for protein immobilization. *Langmuir* **2007**, *23*, 4465–4471.

(9) Asakawa, K.; Tahara, S.; Nakamichi, M.; Takehara, K.; Ikeno, S.; Linder, M.; Haruyama, T. The amphiphilic protein HFBII as a genetically taggable molecular carrier for the formation of a self-organized functional protein layer on a solid surface. *Langmuir* **2009**, *25*, 8841–8844.

(10) Linder, M.; Szilvay, G. R.; Nakari-Setälä, T.; Söderlund, H.; Penttilä, M. Surface adhesion of fusion proteins containing the hydrophobins HFBI and HFBII from Trichoderma reesei. *Protein Sci.* **2002**, *11*, 2257–2266.

(11) Lumsdon, S. O.; Green, J.; Stieglitz, B. Adsorption of hydrophobin proteins at hydrophobic and hydrophilic interfaces. *Colloids Surf., B* **2005**, *44*, 172–178.

(12) Li, X.; Hou, S.; Feng, X.; Yu, Y.; Ma, J.; Li, L. Patterning of neural stem cells on poly(lactic-co-glycolic acid) film modified by hydrophobin. *Colloids Surf., B* **2009**, *74*, 370–374.

(13) Tchuenbou-Magaia, F. L.; Norton, I. T.; Cox, P. W. Hydrophobins stabilised air-filled emulsions for the food industry. *Food Hydrocolloids* **2009**, *23*, 1877–1885.
(14) Blijdenstein, T. B. J.; de Groot, P. W. N.; Stoyanov, S. D. On the link between foam coarsening and surface rheology: why hydrophobins are so different. *Soft Matter* **2010**, *6*, 1799–1808.
(15) Wessels, J. G. H. Developmental regulation of fungal cell-wall formation. *Annu. Rev. Phytopathol.* **1994**, *32*, 413–437.
(16) Nakari-Setälä, T.; Aro, N.; Kalkkinen, N.; Alatalo, E.; Penttilä, M. Genetic and biochemical characterization of the Trichoderma reesei hydrophobin HFBI. *Eur. J. Biochem.* **1996**, *235*, 248–255.
(17) Nakari-Setälä, T.; Aro, N.; Ilmén, M.; Muñoz, G.; Kalkkinen, N.; Penttilä, M. Differential expression of the vegetative and spore-bound hydrophobins of Trichoderma reesei — cloning and characterization of the HFBII gene. *Eur. J. Biochem.* **1997**, *248*, 415–423.
(18) Kisko, K.; Szilvay, G. R.; Vuorimaa, E.; Lemmetyinen, H.; Linder, M. B.; Torkkeli, M.; Serimaa, R. Self-assembled films of hydrophobin protein HFBIII from Trichoderma reesei. *J. Appl. Crystallogr.* **2007**, *40*, s355–s360.
(19) Torkkeli, M.; Serimaa, R.; Ikkala, O.; Linder, M. Aggregation and self-assembly of hydrophobins from Trichoderma reesei: low-resolution structural models. *Biophys. J.* **2002**, *83*, 2240–2247.
(20) Szilvay, G. R.; Nakari-Setälä, T.; Linder, M. B. Behavior of Trichoderma reesei hydrophobins in solution:interactions, dynamics, and multimer formation. *Biochemistry* **2006**, *45*, 8590–8598.
(21) Kisko, K.; Szilvay, K. R.; Vainio, U.; Linder, M. B.; Serimaa, R. Interactions of Hydrophobin Proteins in Solution Studied by Small-Angle X-Ray Scattering. *Biophys. J.* **2008**, *94*, 198–206.
(22) Kisko, K.; Szilvay, G. R.; Vuorimaa, E.; Lemmetyinen, H.; Linder, M. B.; Torkkeli, M.; Serimaa, R. Self-assembled films of hydrophobin proteins HFBI and HFBII studied in situ at the air/water interface. *Langmuir* **2009**, *25*, 1612–1619.
(23) Wang, X.; Graveland-Bikker, J. F.; de Kruif, C. G.; Robillard, G. T. Oligomerization of hydrophobin SC3 in solution: From soluble state to self-assembly. *Protein Sci.* **2004**, *13*, 810–821.
(24) Kisko, K.; Torkkeli, M.; Vuorimaa, E.; Lemmetyinen, H.; Seeck, O. H.; Linder, M.; Serimaa, R. Langmuir—Blodgett films of hydrophobins HFBI and HFBII. *Surf. Sci.* **2005**, *584*, 35–40.
(25) Askolin, S.; Linder, M.; Scholtmeijer, K.; Tenkanen, M.; Penttila, M.; de Vocht, M. L.; Wosten, H. A. B. Interaction and comparison of a class I hydrophobin from Schizophyllum commune and class II hydrophobins from Trichoderma reesei. *Biomacromolecules* **2006**, *7*, 1295–1301.
(26) Szilvay, G. R.; Paananen, A.; Laurikainen, K.; Vuorimaa, E.; Lemmetyinen, H.; Peltonen, J.; Linder, M. B. Self-assembled hydrophobin protein films at the air-water interface: structural analysis and molecular engineering. *Biochemistry* **2007**, *46*, 2345–2354.
(27) Hakanpää, J.; Paananen, A.; Askolin, A.; Nakari-Setälä, T.; Parkkinen, T.; Penttilä, M.; Linder, M. B.; Rouvinen, J. Atomic resolution structure of the HFBII hydrophobin, a self-assembling amphiphile. *J. Biol. Chem.* **2004**, *279*, 534–539.
(28) Basheva, E. S.; Kralchevsky, P. A.; Danov, K. D.; Stoyanov, S. D.; Blijdenstein, T. B. J.; Pelan, E. G.; Lips, A. Self-assembled bilayers from the protein HFBII hydrophobin: nature of the adhesion energy. *Langmuir*, submitted.
(29) Bailey, M.; Askolin, S.; Hörhammer, N.; Tenkanen, M.; Linder, M.; Penttilä, M.; Nakari-Setälä, T. Process technological effects of deletion and amplification of hydrophobins I and II in transformants of Trichoderma reesei. *Appl. Microbiol. Biotechnol.* **2002**, *58*, 721–727.
(30) Lopes, T. S.; de Wijs, I. J.; Steenhauer, S. I.; Verbakel, J.; Planta, R. J. Factors affecting themitotic stability of high-copy-number integration into the ribosomal DNA of Saccharomyces cerevisiae. *Yeast* **1996**, *12*, 467–477.
(31) Thomassen, Y. E.; Meijer, W.; Sierkstra, L.; Verrips, C. T. Large-scale production of VHH antibody fragments by Saccharomyces cerevisiae. *Enzyme Microb. Technol.* **2002**, *30*, 273–278.
(32) Scheludko, A.; Exerowa, D. Instrument for interferometric measurements of the thickness of microscopic foam films. *C. R. Acad. Bulg. Sci.* **1959**, *7*, 123–132.
(33) Scheludko, A. Thin liquid films. *Adv. Colloid Interface Sci.* **1967**, *1*, 391–464.
(34) Wierenga, P. A.; Basheva, E. S.; Denkov, N. D. Modified capillary cell for foam film studies allowing exchange of the film—forming liquid. *Langmuir* **2009**, *25*, 6035–6039.
(35) Kralchevsky, P. A.; Nagayama, K. *Particles at Fluid Interfaces and Membranes*; Elsevier: Amsterdam, 2001; Chapter 14.
(36) Dushkin, C. D.; Yoshimura, H.; Nagayama, K. Nucleation and growth of two-dimensional colloidal crystals. *Chem. Phys. Lett.* **1993**, *204*, 455–460.
(37) Bachilo, S. M.; Strano, M. S.; Kittrell, C.; Hauge, R. H.; Smalley, R. E.; Weisman, R. B. Structure-assigned optical spectra of single-walled carbon nanotubes. *Science* **2002**, *298*, 2361–2366.
(38) Geim, A. K.; Novoselov, K. S. The rise of graphene. *Nature Mater.* **2007**, *6*, 183–191.
(39) Geim, A. K. Graphene: status and prospects. *Science* **2009**, *324*, 1530–1534.
(40) Macosko, C. W. *Rheology: Principles, Measurements and Applications*; Wiley-VCH: New York, 1994; Chapter 2.5.
(41) Malkin, A. Ya. *Rheology Fundamentals*; ChemTec Publishing: Toronto, 1994; p 66.
(42) Steffe, J. F. *Rheological Methods in Food Process Engineering*, 2nd ed.; Freeman Press: East Lancing, MI, 1996; Chapter 1.6.
(43) Petkov, J. T.; Gurkov, T. D.; Campbell, B. E. Measurement of the yield stress of gellike protein layers on liquid surfaces by means of an attached particle. *Langmuir* **2001**, *17*, 4556–4563.
(44) Petkov, J. T.; Gurkov, T. D.; Campbell, B. E.; Borwankar, R. P. Dilatational and shear elasticity of gel-like protein layers on air/water interface. *Langmuir* **2000**, *16*, 3703–3711.
(45) Freer, E. M.; Yim, K. S.; Fuller, G. G.; Radke, C. J. Shear and dilatational relaxation mechanisms of globular and flexible proteins at the hexadecane/water interface. *Langmuir* **2004**, *20*, 10159–10167.
(46) Gasteiger, E.; Hoogland, C.; Gattiger, A.; Duvaud, S.; Wilkins, M. R.; Appel, R. D.; Bairoch, A. Protein identification and analysis tools on the ExPASy server. In *The Proteomics Protocols Handbook*; Walker, J. M., Ed.; Humana Press: Totowa, NJ, 2005; pp 571—607.
(47) Basheva, E. S.; Gurkov, T. D.; Christov, N. C.; Campbell, B. Interactions in oil/water/oil films stabilized by β-lactoglobulin; role of the surface charge. *Colloids Surf., A* **2006**, *282*, 99–108.
(48) Khristov, K.; Czarnecki, J. Emulsion films stabilized by natural and polymeric surfactants. *Curr. Opin. Colloid Interface Sci.* **2010**, *15*, 324–329.
(49) Saccani, J.; Castano, S.; Beaurain, F.; Laguerre, M.; Desbat, B. Stabilization of phospholipid multilayers at the air-water interface by compression beyond the collapse. *Langmuir* **2004**, *20*, 9190–9197.
(50) Mallouri, R.; Keramidas, A. D.; Brezesinski, G.; Leontidis, E. Monolayer properties of surface-active metalorganic complexes with a tunable headgroup. *J. Colloid Interface Sci.* **2008**, *317*, 544–555.
(51) van der Linden, E.; Versluis, P. Membrane crumpling and restricted swelling in onion phases. *Physica A* **2001**, *298*, 75–80.
(52) Horozov, T. S.; Binks, B. P.; Aveyard, R.; Clint, J. H. Effect of particle hydrophobicity on the formation and collapse of fumed silica particle monolayers at the oil—water interface. *Colloids Surf., A* **2006**, *282*, 377–386.
(53) Danov, K. D.; Kralchevsky, P. A.; Stoyanov, S. D. Elastic Langmuir layers and membranes subjected to unidirectional compression: wrinkling and collapse. *Langmuir* **2010**, *26*, 143–155.
(54) Fernandez-Puente, L.; Bivas, I.; Mitov, M. D.; Méléard, P. Temperature and chain length effects on bending elasticity of phosphatidylcholine bilayers. *Europhys. Lett.* **1994**, *28*, 181–186.
(55) Méléard, P.; Gerbeaud, C.; Pott, T.; Fernandez-Puente, L.; Bivas, I.; Mitov, M. D.; Dufourcq, J.; Bothorel, P. Bending elasticities of model membranes: influences of temperature and sterol content. *Biophys. J.* **1997**, *72*, 2616–2629.
(56) Méléard, P.; Gerbeaud, C.; Bardusco, P.; Jeandaine, N.; Mitov, M. D.; Fernandez-Puente, L. Mechanical properties of model membranes studied from shape transformations of giant vesicles. *Biochimie* **1998**, *80*, 401–413.

(57) Evans, E. A.; Skalak, R. Mechanics and thermodynamics of biomembranes. Part 1. *CRC Crit. Rev. Bioeng.* **1979**, *3*, 181–330.
(58) Russev, S. C.; Alexandrov, N.; Marinova, K. G.; Danov, K. D.; Denkov, N. D.; Lyutov, L.; Vulchev, V.; Bilke-Krause, C. Instrument and methods for surface dilatational rheology measurements. *Rev. Sci. Instrum.* **2008**, *79*, 104102.
(59) Alexandrov, N.; Marinova, K. G.; Danov, K. D.; Ivanov, I. B. Surface dilatational rheology measurements for oil/water systems with viscous oils. *J. Colloid Interface Sci.* **2009**, *339*, 545–550.
(60) McClements, D. J. Protein-stabilized emulsions. *Curr. Opin. Colloid Interface Sci.* **2004**, *9*, 305–313.
(61) Onsaard, E.; Vittayanont, M.; Srigam, S.; McClements, D. J. Properties and stability of oil-in-water emulsions stabilized by coconut skim milk proteins. *J. Agric. Food Chem.* **2005**, *53*, 5747–5753.
(62) Koczo, K.; Nikolov, A. D.; Wasan, D. T.; Borwankar, R. P.; Gonsalves, A. Layering of sodium caseinate submicelles in thin liquid films - a new stability mechanism for food dispersions. *J. Colloid Interface Sci.* **1996**, *178*, 694–702.
(63) Tcholakova, S.; Denkov, N. D.; Ivanov, I. B.; Campbell, B. Coalescence stability of emulsions containing globular milk proteins. *Adv. Colloid Interface Sci.* **2006**, *123*, 259–293.
(64) Rullier, B.; Axelos, M. A. V.; Langevin, D.; Novales, B. Beta-lactoglobulin aggregates in foam films: correlation between foam films and foaming properties. *J. Colloid Interface Sci.* **2009**, *336*, 750–755.
(65) Rullier, B.; Axelos, M. A. V.; Langevin, D.; Novales, B. Beta-lactoglobulin aggregates in foam films: effect of the concentration and size of the protein aggregates. *J. Colloid Interface Sci.* **2010**, *343*, 330–337.
(66) Dickinson, E. Food emulsions and foams: stabilization by particles. *Curr. Opin. Colloid Interface Sci.* **2010**, *15*, 40–49.
(67) von Klitzing, R.; Thormann, E.; Nylander, T.; Langevin, D.; Stubenrauch, C. Confinement of linear polymers, surfactants, and particles between interfaces. *Adv. Colloid Interface Sci.* **2010**, *155*, 19–31.
(68) Messner, P.; Sleytr, U. Crystalline bacterial cell-surface layers. *Adv. Microb. Physiol.* **1992**, *33*, 213–275.
(69) Paananen, A.; Vuorimaa, E.; Torkkeli, M.; Penttilä, M.; Kauranen, M.; Ikkala, O.; Lemmetyinen, H.; Serimaa, R.; Linder, M. B. Structural hierarchy in molecular films of two class II hydrophobins. *Biochemistry* **2003**, *42*, 5253–5258.
(70) Israelachvili, J. N. *Intermolecular and Surface Forces*; Academic Press: London, 1992.
(71) Marinova, K. G.; Gurkov, T. D.; Velev, O. D.; Ivanov, I. B.; Campbell, B.; Borwankar, R. P. The role of additives for the behaviour of thin emulsion films stabilized by proteins. *Colloids Surf., A* **1997**, *123*, 155–167.
(72) Wang, Z.; Lienemann, M.; Qiau, M.; Linder, M. B. Mechanisms of protein adhesion on surface films of hydrophobin. *Langmuir* **2010**, *26*, 8491–8496.
(73) Popa, I.; Gillies, G.; Papastavrou, G.; Borkovec, M. Attractive electrostatic forces between identical colloidal particles induced by adsorbed polyelectrolytes. *J. Phys. Chem. B* **2009**, *113*, 8458–8461.